

EXPLORING LARGE-SCALE STRUCTURE WITH BILLIONS OF GALAXIES

HU ZHAN, LLOYD KNOX, ANTHONY TYSON, AND VERA MARGONINER
 Department of Physics, University of California, Davis, CA 95616
Draft version April 10, 2019

ABSTRACT

We consider cosmological applications of galaxy number density correlations to be inferred from future deep and wide multi-band optical surveys. We mostly focus on very large scales as a probe of possible features in the primordial power spectrum. We find the proposed survey of the Large Synoptic Survey Telescope may be competitive with future all-sky CMB experiments over a broad range of scales. On very large scales the inferred power spectrum is robust to photometric redshift errors, and, given a sufficient number density of galaxies, to angular variations in dust extinction and photometric calibration errors. We also consider other applications, such as constraining dark energy with the two CMB-calibrated standard rulers in the matter power spectrum, and controlling the effect of photometric redshift errors to facilitate the interpretation of cosmic shear data. We find that deep photometric surveys over wide area can provide constraints that are competitive with spectroscopic surveys in small volumes.

Subject headings: cosmology: theory — dark matter — galaxies: clusters: general — gravitational lensing — large-scale structure of universe

1. INTRODUCTION

Results from the *Wilkinson Microwave Anisotropy Probe* (*WMAP*, Bennett et al. 2003) have revealed a CMB temperature power spectrum that is remarkably well-fit by a simple 5 or 6-parameter model (e.g. Spergel et al. 2003). The success of this simple model is somewhat qualified by irregularities on large scales. There is evidence for departures from statistical isotropy, an anomalously low quadrupole amplitude, an anomalous absence of correlations on angular scales greater than 60 degrees, non-Gaussianity, and sharp features in the temperature power spectrum (Luminet et al. 2003; Peiris et al. 2003; de Oliveira-Costa et al. 2004; Efstathiou 2004; Eriksen et al. 2004b; Hansen et al. 2004; Schwarz et al. 2004; Land & Magueijo 2005; Jaffe et al. 2005). While these irregularities may eventually be revealed to be due to improper modeling of the instrument or astrophysical foregrounds, they certainly have served to call attention to the possibility of interesting departures from the standard paradigm on the largest observable scales. In this paper we explore how well these scales can be probed by forthcoming deep and wide photometric redshift surveys such as the survey of the Large Synoptic Survey Telescope¹ (LSST).

We find that very large-volume photometric redshift surveys can probe these large scales quite well. For a sufficiently large volume the galaxy power spectra not only provide a complementary look at structure on very large scales, but they can also determine the power spectrum on a given scale even more precisely than with CMB temperature anisotropy measurements. The reason is that in determining a power spectrum one is fundamentally limited by the number of modes on a given scale, and there are more such modes with a three-dimensional sur-

vey than with a two-dimensional survey that encloses the three-dimensional survey.

Determining the power spectrum of the fluctuations on very large scales is of great interest for several reasons. First and foremost, the power spectrum on these scales can be cleanly used to infer the power spectrum of primordial fluctuations, and the primordial fluctuation power spectrum on any scale is of interest. The primordial power spectrum is one of our only handles on the mechanism that led to the fluctuations that are responsible for the diversity of structures we see in the Universe today, including ourselves.

In the context of inflation, probing larger scales means probing inflation at an earlier epoch. Larger scales exited the fixed-size horizon earlier and thus had more time to expand. Reaching back to these earlier epochs may provide us with valuable clues about inflation.

Finally, exploring these large scales is perhaps the best way, other than precision measurement of CMB polarization on large angular scales, to test the claims of statistical anisotropy in the *WMAP* temperature maps.

Others have suggested ways to follow up on the large-scale *WMAP* irregularities. To shed further light on the largest-scale irregularity of all, the low quadrupole amplitude, Doré, Holder, & Loeb (2004) and Skordis & Silk (2004) have proposed to use polarization data. Kesden, Kamionkowski, & Cooray (2003) have proposed to use all-sky cosmic shear measurements. We must also note that the low quadrupole on the sky is actually not that unlikely in a Λ CDM model, and could simply be a statistical fluctuation (Bridle et al. 2003; Cline, Crotty, & Lesgourgues 2003; Contaldi et al. 2003; Gaztañaga et al. 2003; O’Dwyer et al. 2004). More conservative foreground modeling also reduces the level of discrepancy (Eriksen et al. 2004a; Slosar & Seljak 2004). There are also statistical analyses with results that are consistent with statistical isotropy (Hajian, Souradeep, & Cornish 2005).

When independent measurements of the cosmic shear

Electronic address: zhan@physics.ucdavis.edu
 Electronic address: lknox@physics.ucdavis.edu
 Electronic address: tyson@physics.ucdavis.edu
 Electronic address: vem@physics.ucdavis.edu

¹ see <http://www.lsst.org>.

and galaxy power spectrum are combined, one can obtain robust constraints on dark energy (Hu & Jain 2004). Furthermore, Pen (2004) showed explicitly that with a determination of the galaxy power spectra as a function of redshift, one can then indirectly infer the cosmic shear power spectrum with a lower statistical uncertainty than one can directly from the shear maps. While the LSST survey will sharply address dark energy via cosmic shear tomography of billions of galaxies, here we emphasize using galaxy photometry (not shear) in that survey to determine the matter power spectrum.

Deep and wide surveys are not only critical for measuring the power spectrum on very large scales, they also lead to reduced sample variance errors for power spectrum measurements on smaller scales. We therefore consider applications of intermediate-scale constraints on the power spectrum as well. Namely, the broadband shape and baryon acoustic oscillations (Peebles & Yu 1970; Bond & Efstathiou 1984; Holtzman 1989; Hu & Sugiyama 1996) in the matter power spectrum can serve as standard rulers to determine the angular diameter distance $r(z)$ and to constrain cosmological parameters (Eisenstein, Hu, & Tegmark 1998; Cooray, Hu, Huterer, & Joffre 2001; Hu & Haiman 2003; Linder 2003; Seo & Eisenstein 2003). We find the LSST survey capable of $\sim 1\%$ distance measurements to redshifts between 0.2 and 3.

The paper is organized as follows. Section 2 describes our fiducial survey: the proposed LSST survey. The errors on the matter power spectrum are forecast in Section 3, where effects of photometric redshift errors, redshift distortion, and spherical survey geometry are illustrated. We demonstrate in Section 4 that galaxy counts from the fiducial survey can be used to determine the differential extinction and photometry errors so that these errors do not significantly contaminate the power spectrum. Section 5 shows that comparable precision on the matter power spectrum can be achieved by the LSST and CMB, and that one can measure angular-diameter distances to percent level precision from baryon acoustic oscillations with the LSST. We conclude in Section 6 with remarks on several challenges to measuring the matter power spectrum from photometric galaxy redshift surveys. A brief summary of the spherical harmonic analysis, which is convenient for the survey geometry, is given in the Appendix.

2. FIDUCIAL SURVEY

The LSST will image 23,000 square degrees at high galactic latitude deeply in 5–6 wavelength bands from 0.3–1.1 microns (*grizy* system). Each band will have several hundred 15-second exposures. Given its wide coverage and survey depth, the LSST is ideal for measuring the galaxy power spectrum on very large scales. To estimate the galaxy redshift distribution for the 23,000 square degree survey we degrade the Hubble Deep Field North (HDF-N), which has well-measured redshifts, to match LSST depth and image quality.

We approximate LSST’s filter system using deep HST imaging and ground-based *J*-band ($\lambda_{\text{central}} \sim 13000 \text{ \AA}$) imaging from the 4-m KPNO telescope. First, we convolve the HDF-N UBVJ space images (Williams et al. 1996) with a 0.8” FWHM Gaussian to simulate the worst case seeing conditions. Then, we re-pixelize, add noise,

and catalog the images to match the expected data quality for the final full-depth stack of $500 \times 15\text{s}$ coadded exposures. For example, the final stack will go to 26.7 mag and 25.4 mag (10 and 30σ) in the *i* band. The *J*-band image is left unchanged, because it has the same resolution and worse seeing than expected for LSST.

We then compute photometric redshifts for all detected objects using a technique based on SED fitting, and on a magnitude prior (Margoniner 2005, in preparation). The density of objects is $\sim 250,000$ per square degree. Because we need galaxies with well-determined redshifts, we choose to keep only the ones with a sharp and well-defined peak in its redshift probability distribution; i.e., we require that the width of the peak be less than $0.04(1+z)$. The resulting rms photometric redshift error is somewhat larger than this threshold width of the redshift peak. Our final object density after this cut is $\sim 130,000$ per square degree, with a redshift distribution $\bar{n}_g(z)$ parameterized as:

$$\bar{n}_g(z) = 530z^2 e^{-z/0.32} \text{ arcmin}^{-2}. \quad (1)$$

This exercise results in an rms of $\sigma_z = 0.065(1+z)$. We take this as a conservative upper limit to the rms and adopt $\sigma_z = 0.04(1+z)$ as our fiducial value, which may be achievable by further color-based cuts or priors, although this has yet to be demonstrated. Other surveys have achieved similar accuracy. For example, with luminous red galaxies from the Sloan Digital Sky Survey (SDSS), Padmanabhan et al. (2005) find that $\sigma_z \sim 0.03$ for $z < 0.55$ and ~ 0.06 for $z < 0.7$. We also assume that the photometric redshift bias is calibratable to $0.001(1+z)$. This is possible in each redshift bin using current facilities and spectrographs.

3. MEASURING THE MATTER POWER SPECTRUM

On large scales, the cosmic density field can be approximated by a Gaussian random field. At redshift z , the variance of the Fourier transform of the galaxy number density contrast is

$$\langle \delta_g(\mathbf{k}) \delta_g^*(\mathbf{k}) \rangle = P_g(\mathbf{k}) = b^2(z) g^2(z) P(k) + \bar{n}_g^{-1}, \quad (2)$$

where $P_g(\mathbf{k})$ is the galaxy power spectrum, $P(k)$ the matter power spectrum at $z = 0$, $b(z)$ the galaxy bias, and $g(z)$ the growth factor. We have ignored redshift distortion in equation (2) for the moment. If the factors multiplying $P(k)$ in the above equation are known, each Fourier mode of the density contrast can be used to make a very rough estimate of $P(k)$.

An unknown scale-dependent and stochastic bias will limit our ability to determine the matter power spectrum. However, the galaxy bias is thought to be scale-independent and deterministic on large scales. This expectation has been confirmed for $0.02 h \text{ Mpc}^{-1} < k < 0.1 h \text{ Mpc}^{-1}$ from the power spectrum analysis of the SDSS galaxies (Tegmark et al. 2004), although the bias increases with luminosity. Extensive studies with the halo model, weak lensing, and simulations (Peacock & Smith 2000; Hoekstra et al. 2002; Weinberg et al. 2004; Seljak et al. 2005) will help us better understand the limits of galaxy bias. Here, we assume that the bias is known and scale-independent.

3.1. Procedures

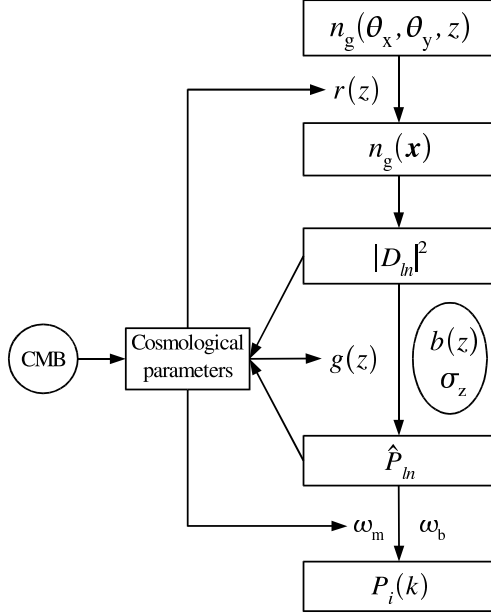


FIG. 1.— Procedures for measuring the large-scale matter power spectrum with the LSST survey.

Measuring the three-dimensional power spectrum on giga-parsec scales brings about two unique issues.

First, one needs the comoving distance $r(z)$ and co-moving angular diameter distance to convert the galaxy number density in redshift and angular coordinates to that in distance coordinates. We assume hereafter that the curvature is known so that only one distance is needed. For a shallow survey at low redshift, Hubble's law suffices to provide an approximation of $r(z)$, but for a survey that reaches $z = 2.5$ one must assume a cosmological model to calculate $r(z)$, or, possibly, obtain it from baryon acoustic oscillations.

Second, because galaxies are observed on a very long light-cone, there is considerable evolution of the bias and density fluctuations within the survey. If not accounted for, this evolution will contaminate the inferred power spectrum on scales (along the light-cone) over which the bias or growth factor changes appreciably.

For a photometric survey, there is yet another issue, namely, the photometric redshift error. It suppresses the power spectrum in a similar way as the pairwise velocity dispersion but with greater magnitude.

To summarize, we outline in Fig. 1 the procedures of measuring the matter power spectrum with the LSST survey. The survey provides the galaxy number density $n_g(\theta_x, \theta_y, z)$, which is converted to $n_g(x)$ with the knowledge of $r(z)$ from a specific cosmological model determined by the CMB or from baryon oscillations. The raw three-dimensional galaxy power spectrum $|D_{ln}|^2$ can then be calculated. The subscripts ln are the result of the spherical harmonic analysis (see the Appendix). This raw power spectrum is strongly suppressed in the radial direction. With a proper modeling of the effect of photometric redshift errors, redshift distortions, and galaxy bias one can estimate the changing rate of the growth function, $d \ln g / d \ln a$, which may be approximated by $\Omega_m^{0.6}$ (Lahav et al. 1991). After the above correction, one obtains an estimate of the three-dimensional matter

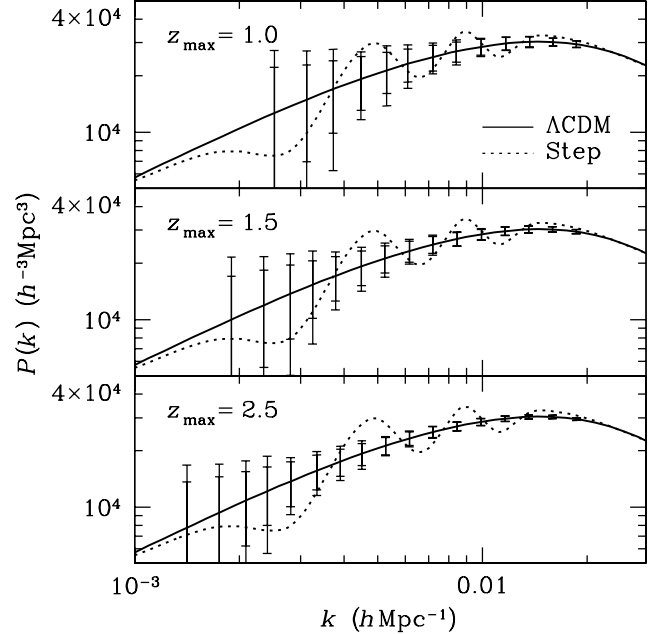


FIG. 2.— Effect of depth (z_{\max}) on error forecasts for measurements of the matter power spectrum with the LSST. A 23,000 square degree photometric galaxy redshift survey is assumed. The solid line is the fiducial model power spectrum, while the dotted line is the power spectrum generated by the step inflation potential (Peiris et al. 2003). The error bars are 1σ dispersions of the power spectrum measured in non-overlapping logarithmic bins with bin width $\Delta k \simeq 0.16k$. The inner error bars are based on the simple mode-counting in a cubic volume, e.g. equation (4), while the outer ones count spherical harmonic modes using equation (7). All the power spectra are scaled to $z = 0$.

power spectrum \hat{P}_{ln} . Cosmological parameters can be estimated from \hat{P}_{ln} through the features imprinted in it and be fed back to the beginning of the procedures. Finally, the primordial matter power spectrum $P_i(k)$ can be reconstructed from \hat{P}_{ln} with inputs of the matter density ω_m and baryon density ω_b and compared with that from the CMB (e.g. Bridle et al. 2003).

3.2. Forecasting Errors on $P(k)$

For simplicity, and because we are only interested in the largest scales, we drop the negligible shot-noise term, as justified below. Thus, the standard error in $P(k)$ estimated from modes within a band of width Δk is simply

$$\sigma_P(k) = \sqrt{2/N_k} P(k), \quad (3)$$

where N_k is the number of independent modes in a shell of width Δk centered at k . For a cubic survey with volume V , N_k is given by

$$N_k = k^2 \Delta k V / 2\pi^2. \quad (4)$$

Variants of these equations can be found in Feldman, Kaiser, & Peacock (1994) and Tegmark (1997). We will see that this simple description of the errors is a good approximation.

To probe the very largest length scales, we want to go as deep as possible. As an example, we show in Fig. 2 the power spectrum of a concordance model consistent with the *WMAP* (Spergel et al. 2003) along with the power spectrum generated by a step inflation potential (Peiris

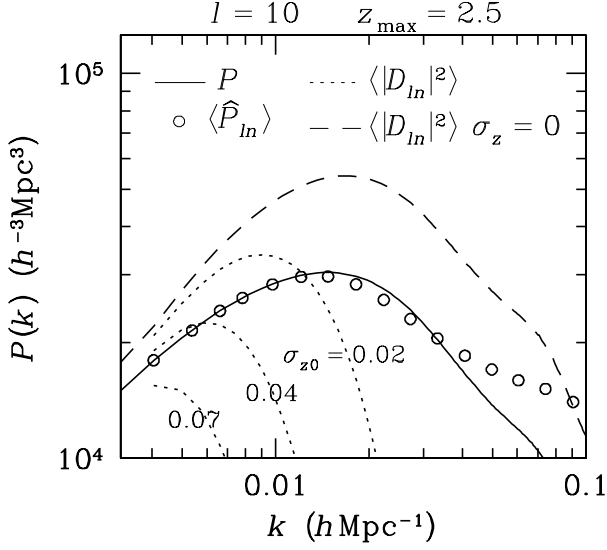


FIG. 3.— Estimated three-dimensional matter power spectrum $\langle \hat{P}_{ln} \rangle$ (circles) for $l = 10$ and $z_{\max} = 2.5$. The solid line is the real-space matter power spectrum. The dotted lines are the redshift-space galaxy power spectrum with the effect of photometric redshift errors and the linear redshift distortion, while the dashed line is the redshift-space galaxy power spectrum with only the linear redshift distortion. The recovered matter power spectrum (circles) is shown for $\sigma_z = \sigma_{z0}(1+z)$ with $\sigma_{z0} = 0.04$; the recovery works better with a smaller σ_{z0} .

et al. 2003). This latter power spectrum provides a better fit to the *WMAP* data. If we cut the fiducial survey at $z_{\max} = 1.0$, then the sample variance in the band power is too large to detect or rule out the step potential. However, it becomes possible when z_{\max} extends to 2.5.

Our description of the errors on $P(k)$ assumes a cubic geometry without redshift distortions or photometric redshift errors. In reality, the survey volumes are wedges from a sphere, with redshift distortions and errors in the radial direction. Spherical harmonic analysis (for details, see the Appendix) is well suited for the real situation. A simple estimator of the matter power spectrum \hat{P}_{ln} can be constructed from spherical harmonic modes D_{lmn} of the observed three-dimensional galaxy distribution:

$$\hat{P}_{ln} = \frac{1}{(2l+1)E_{ln}} \left(\sum_m |D_{lmn}|^2 - N_{ln} \right), \quad (5)$$

where l and m enumerate the usual angular modes of the spherical harmonics $Y_{lm}(\hat{\mathbf{r}})$, n is associated with the radial modes k_{ln} of the spherical Bessel function $j_l(k_{ln}r)$, and N_{ln} is the shot noise. The ensemble average of the estimator is

$$\langle \hat{P}_{ln} \rangle = \frac{1}{E_{ln}} \sum_{n'} U_{lnn'}^2 P(k_{ln'}), \quad (6)$$

where $U_{lnn'}^2$ accounts for photometric redshift errors and the linear redshift distortion, and $E_{ln} = \sum_{n'} U_{lnn'}^2$. We neglect the nonlinear redshift distortion because it behaves in a similar way as the photometric redshift error but has a much smaller effect.

We calculate the three-dimensional redshift-space galaxy power spectrum $\langle |D_{ln}|^2 \rangle = \langle |D_{lmn}|^2 \rangle_m$ using equation (A5) and recover the real-space matter power spectrum $\langle \hat{P}_{ln} \rangle$ using the simple estimator equation (6).

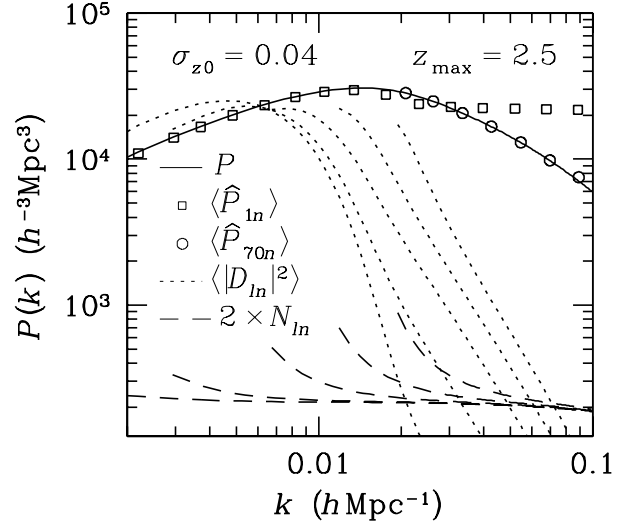


FIG. 4.— Similar to Fig. 3, but we show the three-dimensional redshift-space galaxy power spectrum $\langle |D_{ln}|^2 \rangle$ and recovered matter power spectrum $\langle \hat{P}_{ln} \rangle$ for different multipoles. From left to right, the redshift-space galaxy power spectrum (dotted lines) and shot noise N_{ln} (dashed lines) are calculated with $l = 1, 6, 20, 40$, and 70. The matter power spectrum $\langle \hat{P}_{ln} \rangle$ is estimated with $l = 1$ (squares) and 70 (circles). The redshift-space galaxy power spectrum increases with the multipole number on scales dominated by photometric redshift errors, because at the same wavenumber higher multipoles contain a smaller fraction of radial modes, which are affected by photometric redshift errors, and a larger fraction of angular modes, which are not.

The results are shown in Fig. 3 for $l = 10$ and $z_{\max} = 2.5$. The redshift-space galaxy power spectrum (dotted lines) is strongly suppressed by photometric redshift errors at $k \gtrsim H(z)/c\sigma_z$,² while the simple estimator $\langle \hat{P}_{ln} \rangle$ recovers the matter power spectrum reasonably well at $k \leq 0.02 h \text{ Mpc}^{-1}$ assuming an rms photometric redshift error of $\sigma_{z0} = 0.04$. The discrepancies between the recovered and actual matter power spectra at $k > 0.02 h \text{ Mpc}^{-1}$ are due to the broadening of the window function $U_{lnn'}^2$ at high wavenumbers and our use of the very simple estimator. More sophisticated estimators can be designed to improve the accuracy of the recovery. For $\sigma_{z0} = 0.02$, there will be no discernible difference between the recovered and the true matter power spectra within the range of Fig. 3.

Since the correction is so large, one needs to know σ_z accurately to recover the power spectrum. In the (unachievable) case of no redshift errors; i.e., $\sigma_z = 0$, $\langle |D_{ln}|^2 \rangle$ is boosted relative to $P(k)$ by a factor that approaches a constant at larger wavenumbers, where the plane-parallel approximation is valid and the Kaiser (1987) formula applies (Heavens & Taylor 1995).

Examples of different multipoles are given in Fig. 4. One sees that the redshift-space galaxy power spectrum (dotted lines) increases with the multipole number on scales dominated by photometric redshift errors. The reason is that at the same wavenumber higher multipoles contain a smaller fraction of radial modes, which are affected by photometric redshift errors, and a larger fraction of angular modes, which are not. From the difference between multipoles of the redshift-space galaxy power

² We drop the subscripts of the wavenumber for convenience.

spectrum one may actually quantify the effect of photometric redshift errors (and redshift distortions) without knowing σ_z . This is analogous to using the quadrupole-to-monopole ratio to determine the redshift distortion parameter and pairwise velocity dispersion (e.g. Cole, Fisher, & Weinberg 1994; Peacock et al. 2001). The estimated matter power spectrum $\langle \hat{P}_{ln} \rangle$ with $l = 1$ fails to recover the true power spectrum at $k \gtrsim 0.02 h \text{ Mpc}^{-1}$ because the window function $U_{1nn'}^2$ is too broad there to guarantee the accuracy of the simple estimator (note that $U_{70nn'}^2$ remains narrow). This can be improved with a better estimator.

Fig. 4 also demonstrates that the shot noise N_{ln} is indeed negligible on scales of interest for the fiducial survey with $z_{\max} = 2.5$. Since $\bar{n}_g(z)$ increases rapidly with decreasing redshift, the shot noise for a lower z_{\max} is also negligible. The rise of the shot noise at small wavenumbers is due to the radial variation of the selection function as well as the wavenumber-dependence of the weight function [see equation (A6)]. Otherwise, N_{ln} would be wavenumber-independent.

Given that the shot noise is very low, we can divide the galaxies into sub-samples of different luminosity and measure the power spectrum of each sub-sample separately. Although sub-sampling cannot reduce the cosmic variance, one does gain by reducing the inhomogeneity in each sub-sample that is used as a (biased) tracer of the cosmic density field. By comparing the power spectra of luminosity classes, we can infer the relative bias between them (see e.g. Norberg et al. 2001; Zehavi et al. 2002) and test the assumption of a scale-independent bias on large scales.

The estimator \hat{P}_{ln} can be further binned to reduce the error variance. We calculate the window functions $U_{lnn'}^2$ that relate the three-dimensional real-space matter power spectrum to the redshift-space galaxy power spectrum using equation (A6). The $l = 10$ results are shown in Fig. 5. Since the window functions are fairly narrow in k space, each \hat{P}_{ln} is nearly independent of each other. Thus, equation (3) is still valid for forecasting the errors, but the mode counting becomes

$$N_k = f_{\text{sky}} \sum_{l>0} (2l + 1) N_l, \quad (7)$$

where f_{sky} is the fraction of the sky covered by the survey, and N_l is the number of radial modes of multipole l that fall in the band. We have neglected the shot noise and approximated the reduction in the number of modes due to partial sky coverage by an overall reduction of modes by a factor of f_{sky} . For a real survey, one can incorporate the sky cut as well as an angular selection function (or mask) numerically. We exclude the monopole modes, because they can be confused with the radial selection function. Further modifications to equation (7) are needed in the regime where the window function $U_{lnn'}^2$ starts to broaden.

After counting spherical harmonic modes, we find that the spherical geometry only mildly increases the sample variance of $P(k)$ on the scales of interest, which can be identified with the outer error bars in Fig. 2. Hence, the simple mode counting with a cubic geometry can still serve as a reasonable approximation.

4. EXTINCTION AND PHOTOMETRY ERRORS

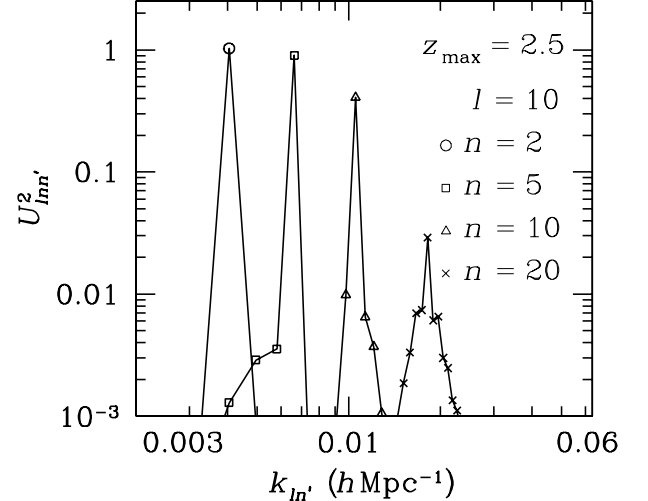


FIG. 5.— The window functions $U_{lnn'}^2$ that relate the three-dimensional real-space matter power spectrum to the redshift-space galaxy power spectrum [see equation (A5)]. They are calculated here with $l = 10$. Symbols also mark the wavenumbers of several discrete modes $k_{ln'}$. They become broader at higher wavenumbers because of photometric redshift errors and redshift distortion. The window functions of other multipoles are similar to those of $l = 10$ but shifted toward higher (lower) wavenumbers for higher (lower) multipoles.

On very large scales, the variance of density fluctuations in logarithmic k bins is very small, e.g. $\Delta^2(k) = k^3 P(k)/2\pi^2 \sim 10^{-3}$ at $k = 0.01 h \text{ Mpc}^{-1}$. An unknown varying extinction over the wide survey area can cause fluctuations in galaxy counts that may swamp the signal. If the logarithmic slope of galaxy counts $\bar{n}_g(< m)$ as a function of magnitude is $s = d \log \bar{n}_g / dm$, then the fractional error in galaxy counts is

$$\frac{\delta n_g}{n_g} = \ln 10 s \delta m = 2.5 s \frac{\delta f}{f}, \quad (8)$$

where $\delta f/f$ is the fractional error in flux caused by, e.g., extinction correction residuals. Observationally s varies from 0.6 at blue wavelengths to 0.3 in the red (e.g. Tyson 1988; Pozzetti et al. 1998; Yasuda et al. 2001), and tends to be flatter for fainter galaxies (Metcalfe et al. 2001; Liske et al. 2003). To keep this systematic angular fluctuation well below $\Delta(k)$, one has to reduce the flux error to 1% or better over the whole survey area. This is a very conservative estimate, because the power spectrum receives contributions from not only angular clustering but also radial clustering of galaxies on large scales, which is much less affected by the extinction or photometry errors.

Extinction A_λ (in mag) is related to reddening via color excess $E(B-V)$. Aside from a zero-point difference of 0.02 mag, the reddening maps made with different methods by Burstein & Heiles (1982) and Schlegel, Finkbeiner, & Davis (1998) agree with each other up to an rms error of 0.007 mag (Burstein 2003). With $A_B = 4.3E(B-V)$, the relative error in reddening translates to an error of 0.03 mag in B magnitude or a flux error of 3%. H I data and galaxy counts were combined to produce the reddening map in Burstein & Heiles (1982). At that time galaxy counts were typically less than 100 per square degree and thus prone to statistical error.

With 250,000 galaxies per square degree³, the LSST will achieve the same accuracy in differential extinction with two-dimensional galaxy counts alone, as long as the dust, or anything that alters the flux, is largely confined in our galaxy, or, at least, at very low redshift.

The number of galaxies N_g within an angular window $\Theta(\hat{\mathbf{r}})$ is given by

$$N_g = \int n_g(\mathbf{r}) \Theta(\hat{\mathbf{r}}) d^3r \quad (9)$$

$$= \int \bar{n}_g(r) \Theta(\hat{\mathbf{r}}) [\delta_g(\mathbf{r}) + 1] d^3r.$$

The mean number counts is

$$\bar{N}_g = \int \bar{n}_g(r) \Theta(\hat{\mathbf{r}}) d^3r, \quad (10)$$

and the variance is

$$\sigma_{N_g}^2 = \sum_{lm} \int P(k) |n_l(k) \Theta_{lm}|^2 k^2 dk, \quad (11)$$

where

$$n_l(k) = \sqrt{\frac{2}{\pi}} \int \bar{n}_g(z) b(z) g(z) j_l(kr) dz,$$

$$\Theta_{lm} = \int \Theta(\hat{\mathbf{r}}) Y_{lm}^*(\hat{\mathbf{r}}) d\hat{\mathbf{r}}.$$

We have used the identities

$$\bar{n}_g(r) r^2 dr = \bar{n}_g(z) dz \quad (12)$$

$$e^{i\mathbf{k}\mathbf{r}} = 4\pi \sum_{lm} i^l j_l(kr) Y_{lm}(\hat{\mathbf{r}}) Y_{l-m}(\hat{\mathbf{k}}) \quad (13)$$

to derive equation (11). The variance of N_g is analogous to the rms density fluctuation within a volume (e.g. Zhan & Fang 2003).

For demonstration purpose, we calculate the variance with an angular window function

$$\Theta(\theta, \phi) \equiv \Theta(\theta) = e^{-\theta^2/2\theta_M^2},$$

where θ and ϕ are, respectively, the polar and azimuthal angles. The multipole number l can be approximately related to the characteristic scale of the window function θ_M by $l \sim 360^\circ/\theta_M$.

For the effect of the galactic extinction, we use the same axial symmetric window function, and place it randomly on the reddening map (Schlegel et al. 1998) with a restriction that its central galactic latitude $|b_c| > 20^\circ + 1.5\theta_M$. The rms fluctuation of B -band galaxy counts within the window function is calculated with the conversion $\delta n_g/n_g \sim \delta A_B = 4.3\delta E(B - V)$.

The results are shown in Fig. 6. The galactic extinction apparently has a dominant effect over galaxy clustering. However, the rms fluctuation due to galaxy clustering does not include radial clustering because of the projection in redshift direction. When the radial information is restored, the clustering variance will be much higher. If one restricts the window function to higher galactic latitude, the rms fluctuation due to extinction will be

³ Since the two-dimensional projection of galaxy counts does not require redshift information, one can use all galaxies that have good photometry.

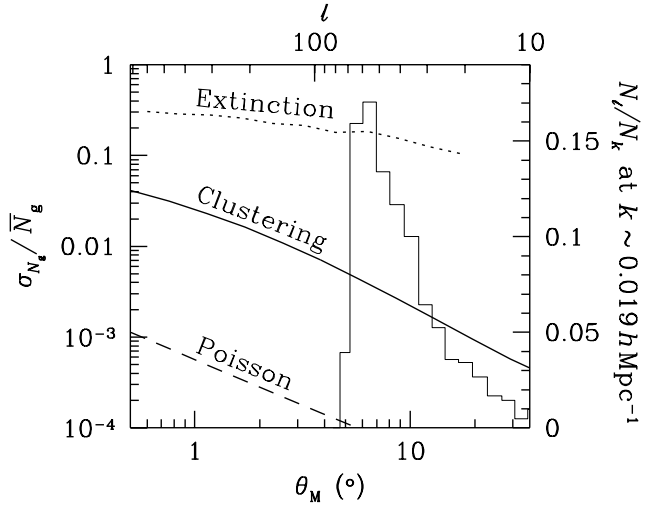


FIG. 6.— Rms fluctuations of galaxy counts due to the extinction (dotted line), galaxy clustering (solid line), and Poisson noise $1/\sqrt{N_g}$ (dashed line) within an angular window of size θ_M . The histogram shows the contribution to the number of independent modes N_k ($k \sim 0.019 h \text{ Mpc}^{-1}$) from each band of multipoles for the highest waveband in Fig. 2. The scale of the histogram is marked on the right axis. For lower wavebands, the distribution moves to lower multipoles. The multipole number l is related to θ_M by $l \sim 360^\circ/\theta_M$.

smaller. In addition, one can also correct for the fluctuations in the extinction; what will hinder the measurement of the galaxy power spectrum is rather the uncertainties in the extinction.

If one attributes all the angular variations in the projected galaxy surface number density to extinction (or any form of photometry errors), the rms residual of relative flux error will be set by the intrinsic rms fluctuation of the projected galaxy number density due to clustering, which is well below 1% on scales above several degrees, where the contribution to N_k ($k \sim 0.019 h \text{ Mpc}^{-1}$) peaks. For smaller ks (larger scales), the contribution comes from lower multipoles, and the rms fluctuation of the number counts decreases further. This means that the relative flux error over several square degrees can be controlled to better than 1% by two-dimensional galaxy counts from the LSST, which is sufficiently accurate for measuring the three-dimensional power spectrum on the largest scales.

Further improvement on the relative flux error is possible by combining galaxy counts with multi-band photometry (e.g. Babbedge, Whitaker, & Morris 2005) and H I and CO surveys. Since the Poisson noise in the galaxy counts is an order of magnitude lower than that caused by galaxy clustering, one can also divide the galaxies into groups of similar properties and compare them in one field with those in another to better determine the differential extinction.

5. APPLICATIONS

Determination of the mass power spectrum has many scientific applications. They include searching for dark energy fluctuations, determining the dark energy equation of state, determining the sum of neutrino masses, and probing the primordial power spectrum of fluctuations produced during inflation. Here we consider two ap-

plications: determining the primordial power spectrum to probe inflation and determining the distance-redshift relation in order to probe dark energy.

5.1. The Primordial Power Spectrum of Density Perturbations

The mass power spectrum on large scales is a direct measure of the primordial fluctuations, and it provides a means to probe the generator of these fluctuations. Recent CMB observations have revealed some puzzling properties of the largest scales (Peiris et al. 2003; Efstathiou 2004; Schwarz et al. 2004; de Oliveira-Costa et al. 2004; Eriksen et al. 2004b; Hansen et al. 2004; Land & Magueijo 2005; Jaffe et al. 2005). These peculiar features may very well have their origin in systematic error. However, they have at the very least served to draw attention to the possibility that the very large-scale structure of the Universe may be more complex than in our simplest models.

For specificity, let us focus on one of these puzzles and see how a large-volume photometric redshift survey could shed further light on the solution. In Peiris et al. (2003) it is noted that there are some unusual sharp features, or ‘glitches’, in the rise to the first peak of the WMAP temperature power spectrum. Peiris et al. (2003) also suggest that the glitches may be evidence of features in the primordial power spectrum. Adjusting two parameters of an inflation potential model with a sharp break, or ‘step’ (e.g. Gottlöber, Müller, Starobinsky 1991), they find a significantly better fit to the power spectrum than if they assume a featureless power law. The step inflation model leads to a new physical length scale (the size of the Horizon as the inflation scalar field crosses the feature in its effective potential) that imprints itself on the power spectrum as a series of peaks and troughs.

Peiris et al. (2003) point out that the feature in the primordial power spectrum is detectable in future large-volume redshift surveys. One can indeed see in Fig. 2 that the statistical power is there to map out the wiggles with a high signal-to-noise ratio.

These features are much more pronounced in the matter power spectrum than in the temperature power spectrum. The CMB projection from three dimensions to two dimensions makes them less prominent. In general it is interesting to compare the relative abilities of the CMB and galaxy surveys to constrain the primordial power spectrum.

Before turning to forecasts from CMB data though, let us first refine our forecasts from galaxy survey data at $k > 0.01 h \text{ Mpc}^{-1}$. As seen in Fig. 4, one has to apply a large correction for photometric redshift errors and, to a much less extent, redshift distortions to recover the matter power spectrum at $k \gtrsim 0.01 h \text{ Mpc}^{-1}$. An incorrect probability distribution for the redshift errors can introduce significant errors in the recovered matter power spectrum. Even if the correction is accurately determined, one will still be limited by the shot noise at $k \gtrsim 0.1 h \text{ Mpc}^{-1}$, which is boosted by the correction along with the observed galaxy power spectrum.

To avoid sensitivity to uncertain and large corrections for suppression of power due to photometric redshift errors, we can simply discard modes with a lot of suppression in the radial direction. That is, as discussed in Seo & Eisenstein (2003) and Glazebrook & Blake (2005), we

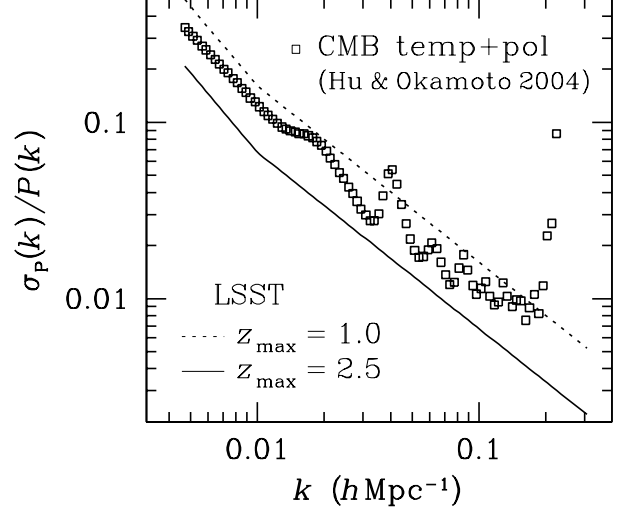


FIG. 7.—Forecasts of sample variance errors on the primordial matter power spectrum. For the LSST, we set $z_{\text{max}} = 1.0$ (dotted line) and 2.5 (solid line), and the mode counting follows equation (14) with $k_{\parallel}^* = 0.01 h \text{ Mpc}^{-1}$. The forecast for the CMB (open squares) includes both temperature and polarization information, and it is taken from Hu & Okamoto (2004). Both forecasts assume a binning of $\Delta k = 0.05k$.

can discard modes with k_{\parallel} above some critical value. The approximate mode counting equation (4) becomes

$$N_k = \begin{cases} k^2 \Delta k V / 2\pi^2 & k_{\parallel} \leq k_{\parallel}^* \\ k k_{\parallel}^* \Delta k V / 2\pi^2 & k_{\parallel} > k_{\parallel}^* \end{cases} \quad (14)$$

where a cubic geometry and the plane-parallel approximation are assumed. One would choose k_{\parallel}^* to be small enough so that residual errors in the power spectrum can be tolerated after correcting for photometric redshift errors and redshift distortion. We set $k_{\parallel}^* = 0.01 h \text{ Mpc}^{-1}$ and assume that the residual error is negligible for $k_{\parallel} \leq k_{\parallel}^*$.

Note that at low k the number of modes scales with k as a three-dimensional survey, increasing as k^3 if $\Delta k \propto k$, and that above k_{\parallel}^* the scaling is that of a two-dimensional survey. Thus, although the CMB will always be the best on length scales larger than those that fit in the galaxy survey, a galaxy survey can compete, at least in terms of the statistical weight, with the CMB on sufficiently small scales. If the cross over scale is large enough, galaxy bias modeling will be simple enough to exploit this statistical improvement.

We present in Fig. 7 the sample variance errors of the primordial matter power spectrum for the LSST with $z_{\text{max}} = 1.0$ (dotted line) and 2.5 (solid line). Also included is the error forecast for the CMB (open squares) using both temperature and polarization information (Hu & Okamoto 2004). It is very encouraging that the LSST can almost match the best-case-scenario CMB results with $z_{\text{max}} = 1.0$ and even provide a better measurement of the primordial power spectrum with $z_{\text{max}} = 2.5$. The cross over scale referred to in the previous paragraph is indeed at very large scales. For the $z_{\text{max}} = 2.5$ case, it is at $k \lesssim 5 \times 10^{-3} h \text{ Mpc}^{-1}$.

The binning in Fig. 7 is for $\Delta k = 0.05k$ for ease of comparison with Hu & Okamoto’s results. However, the spec-

tral resolution of the galaxy survey is $7.5 \times 10^{-4} h \text{ Mpc}^{-1}$ ($z_{\text{max}} = 2.5$) with exceptions for the first few modes of each multipole, which have slightly coarser resolutions. Thus for $k < 0.015 h \text{ Mpc}^{-1}$ the binning assumed in Fig. 7 is too fine. To avoid correlations, that would otherwise increase the errors above the values plotted in the figure, one could bin more coarsely. This coarser binning would *reduce* the level of error below what is plotted in the figure by a factor of $\sqrt{0.05k/\Delta k}$, although the number of points would, of course, be reduced also.

Hu & Okamoto (2004) point out that the CMB power spectrum errors in Fig. 7 are highly correlated and that there are certain linear combinations of the power spectrum measurements with much smaller errors. Approximately 50 principal-component modes of the covariance matrix can be measured to percent level precision. The best-determined principal-component modes are combinations of Fourier powers at $k \gtrsim 0.08 h \text{ Mpc}^{-1}$.

Our forecast for how well the primordial power spectrum can be determined from galaxy survey data is done in the limit of no uncertainty in $r(z)$, $g(z)$, $b(z)$, ω_m and ω_b . We expect that CMB data from *Planck* and the galaxy survey data itself can be used to reconstruct these well enough that the uncertainties do not qualitatively change our error forecasts. The Hu & Okamoto (2004) forecast does include the effect of these uncertainties which are more important for the CMB because of the projection from three dimensions to two dimensions and the greater prominence of the acoustic oscillation features.

We must mention two further caveats. First, for the lowest k values the spherical geometry slightly increases the variance beyond what one gets for a cubic geometry as shown in Fig. 2. Second, whether one can neglect errors in the correction for photometric redshift power suppression at $k < 0.01 h \text{ Mpc}^{-1}$ remains to be demonstrated.

5.2. Standard Rulers For Determining $r(z)$

In the previous subsection we considered how well the primordial power spectrum could be determined with $r(z)$, $g(z)$, $b(z)$, ω_b and ω_m known perfectly. Now we consider how well $r(z)$ can be determined if we assume the primordial power spectrum to be featureless, as expected in the simplest models of inflation. If the power spectrum remained featureless, it would be impossible to reconstruct $r(z)$ from galaxy clustering data, but features imprinted by the evolution of this spectrum can be used as standard rulers for determination of the angular-diameter distance.

In linear perturbation theory there are two length scales that become imprinted on the matter power spectrum. The larger scale feature is the peak near $k = 0.02 h \text{ Mpc}^{-1}$ that can be seen in Fig. 3. The location of this feature depends on the size of the horizon at the epoch of matter-radiation equality. Assuming a standard radiation content, this is set by the matter density, ω_m , which can be determined to sub-percent accuracy with *Planck* (Eisenstein, Hu, & Tegmark 1999). The smaller scale feature is a series of peaks and troughs in the matter power spectrum due to acoustic oscillations the baryons undergo in the pre-recombination plasma (Peebles & Yu 1970; Bond & Efstathiou 1984; Holtzman 1989; Hu & Sugiyama 1996). The length scale here is the comoving

size of the sound horizon at last-scattering. This depends on ω_m and ω_b , which can both be determined well from CMB observations. Thus, both of these features can serve as CMB-calibrated standard rulers, which one can use to determine the comoving angular-diameter distance, $r(z)$ (Eisenstein et al. 1998; Cooray et al. 2001).

Since $r(z) = c \int_0^z dz'/H(z')$ these measurements can be used to map out the history of the expansion rate and thereby provide constraints on the dark energy.

First we will consider the baryonic oscillations. The lowest k peak in the series of baryonic oscillations has already been observed in spectroscopic redshift surveys (Eisenstein et al. 2005; Cole et al. 2005). Several papers have studied how well $r(z)$ and cosmological parameters can be determined from future surveys, both spectroscopic and photometric (Blake & Glazebrook 2003; Hu & Haiman 2003; Linder 2003; Seo & Eisenstein 2003; Blake & Bridle 2004; Dolney, Jain, & Takada 2004; Angulo et al. 2005; Glazebrook & Blake 2005; Linder 2005; Zhan & Knox 2005). Prospects for controlling non-linear evolution and galaxy biasing look very good (White 2005; Seo & Eisenstein 2005). Photometric surveys over larger volumes can provide constraints that are competitive with spectroscopic surveys over smaller volumes.

If one counts the modes using equation (14), the shot noise will continue to be negligible at $k > 0.1 h \text{ Mpc}^{-1}$ and the dominant errors there will come from the uncertainties of the correction for photometric redshift errors, nonlinear redshift distortion, nonlinear evolution, and galaxy bias. Despite the complexities, these errors do not produce oscillating features in the power spectrum. Thus it is possible to use a photometric redshift survey to measure the angular-diameter distance accurately.

We now turn to a discussion of the large-scale feature. Current galaxy surveys cannot be used to measure the power spectrum on scales larger than $k = 0.02 h \text{ Mpc}^{-1}$ due to their limited survey volume. The LSST, on the other hand, will be able to probe scales with wavenumbers as small as several thousandths $h \text{ Mpc}^{-1}$. At the expense of increased sample variance error, one may measure the matter power spectrum in several redshift bins with the LSST. For example, Fig. 7 suggests that 4 equal-volume bins from $z = 0$ to 2.5 will enable us to measure the matter power spectrum to roughly 10% around $k = 0.01 h \text{ Mpc}^{-1}$. The angular scale to which this feature projects depends on the angular-diameter distance to each redshift shell, enabling one to determine the angular-diameter distance.

Generally, constraints from the large-scale feature will be weaker than from the baryonic oscillations for two reasons: first, the latter are much sharper and therefore less tolerant of the horizontal shifts induced by a re-scaling of distances and second, the sample variance errors are larger on larger scales.

However, even this broad feature can lead to powerful distance determinations. Seo & Eisenstein (2003) find that the angular-diameter distance determinations using the large-scale feature have 2 to 3 times larger errors. Thus, though subdominant in their constraining power, the large scale feature offers a useful independent check on distance determination from the baryonic oscillations.

With the LSST and CMB priors from the *Planck* mis-

sion, one can achieve errors of $\sim 1\%$ on $r(z)$, 0.10 on w_0 , and 0.25 on w_a using both the baryon oscillations and broadband feature (Zhan & Knox 2005), where the dark energy equation of state is parametrized as $w(z) = w_0 + w_a[1 - (1 + z)^{-1}]$.

6. DISCUSSION AND CONCLUSIONS

For the reconstruction of the matter power spectrum $P(k)$ to work, we must know the comoving distance $r(z)$, the linear growth function $g(z)$, the galaxy bias $b(z)$, and the rms photometric redshift error σ_z adequately well.

One may improve the knowledge of the galaxy bias on large scales by comparing galaxy statistics with mass statistics inferred from weak lensing (Hoekstra et al. 2002; Seljak et al. 2005), by constructing realistic theoretical models (e.g. Peacock & Smith 2000), and by studying galaxies in large volume hydrodynamical simulations that include star formation and feedback (e.g. Weinberg et al. 2004). Available observational constraints on bias (e.g. Tegmark et al. 2004) constrain it on scales smaller than those of interest here, but since the LSST is designed for weak lensing, it can help to measure the galaxy bias on large scales for galaxies associated with the lensing mass field.

The uncertainties in $r(z)$ and $g(z)$ can be mitigated by assuming a prior for the cosmological model, but at the same time we lose the ability to measure the matter power spectrum model-independently. However, since cosmological information is encoded in the matter power spectrum through multiple channels in addition to $r(z)$ and $g(z)$, cosmological parameters can be estimated from the reconstructed matter power spectrum as well. This will provide a self-consistency check for the choice of the parameters.

Photometric redshift errors strongly suppress the raw galaxy power spectrum $\langle |D_{ln}|^2 \rangle$. Thus, it is crucial to determine the correction for photometric redshift errors. We have adopted a form of this correction from Heavens & Taylor (1995), but other forms also exist (e.g. Ballinger, Peacock, & Heavens 1996). They should be tested against N -body simulations to improve the accuracy. Meanwhile, it appears possible from Fig. 4 that one can infer the correction by comparing the galaxy power spectrum of different multipoles. One may also discard

high k_{\parallel} modes to subdue the errors due to uncertainties in the correction (see Fig. 7).

The extinction is yet another challenge to measuring the matter power spectrum on very large scales. We have demonstrated that with 250,000 projected galaxies per square degree the LSST can actually determine the differential extinction to better than 1% from galaxy counts alone. This means that not only can we be sure that the signal is truly coming from clustering of galaxies but we can also combine the galaxy counts with multi-band photometry (e.g. Babbedge et al. 2005) and H I and CO maps to produce a more accurate reddening map, which will be useful for other observations such as CMB surveys.

Despite all the difficulties, we find that a deep and wide photometric redshift survey, such as can be done with the LSST, can measure the power spectrum of primordial fluctuations on very large scales. The shot noise on these scales is so low (see Fig. 4), that it is possible and beneficial to divide the galaxies into different types to check for consistency and to indirectly test the scale-independence of the galaxy bias on large scales.

The large-scale primordial power spectrum measured from galaxies will complement the CMB experiments and provide valuable insights on inflation. For example, it can be used to examine the possibility of a step inflation potential (Peiris et al. 2003). The large-scale peak and intermediate-scale baryon oscillations in the matter power spectrum will provide useful constraints on cosmological parameters including the dark energy equation of state parameters. They can also reduce the uncertainties of the photometric redshift bias (Zhan & Knox 2005) through the Alcock–Paczynski test (Alcock & Paczynski 1979), and thus prevent the redshift bias from severely degrading the constraining power of the weak lensing tomography on the dark energy equation of state parameters (Huterer et al. 2005; Ma, Hu, & Huterer 2005).

We thank D. Burstein, A. Connolly, D. Eisenstein, and L. Hui for useful conversations about reddening maps, photometric redshift errors, and baryon acoustic oscillations. This work was supported by the National Science Foundation under Grant No. 0307961 and 0441072 and NASA under grant No. NAG5-11098.

APPENDIX

SPHERICAL HARMONIC ANALYSIS

For a survey that covers a large fraction of the sky, the spherical coordinate system is a more suitable basis to work with. The spherical harmonic analysis has been applied to the *IRAS* galaxy catalog (Scharf et al. 1992; Fisher, Scharf, & Lahav 1994), the PSCz galaxy catalog (Tadros et al. 1999), and, recently, the 2dFGRS catalog (Percival et al. 2004). We adopt the formulation in Heavens & Taylor (1995) and describe it here briefly.

The spherical harmonic decomposition of a quantity $A(\mathbf{r})$ is

$$A_{lmn} = c_{ln} \int_0^{r_{\max}} w(r) A(\mathbf{r}) j_l(k_{ln} r) Y_{lm}^*(\hat{\mathbf{r}}) d^3 r, \quad (\text{A1})$$

where an extra weight function $w(r)$ is inserted to minimize the variance in the power spectrum measurement. The discrete wavenumber k_{ln} is the n th root of the boundary condition $d j_l(kr)/dr|_{r_{\max}} = 0$. The normalization c_{ln} satisfies $c_{ln}^{-2} = \int j_l^2(k_{ln} r) r^2 dr$. One can relate the observed three-dimensional galaxy overdensity D_{lmn} to the underlying mass overdensity δ_{lmn} through

$$D_{lmn} = \sum_{n'n''} S_{lnn'} Q_{ln'n''} \delta_{lmn''}, \quad (\text{A2})$$

$$S_{lnn'} = c_{ln} c_{ln'} \int \frac{e^{-(r-y)^2/(2\sigma_z^2)}}{\sqrt{2\pi}\sigma_z} j_l(k_{ln}r) j_l(k_{ln'}y) r dr y dy, \quad (A3)$$

$$Q_{lnn'} = c_{ln} c_{ln'} \int \bar{n}_g(r) g(z) \left\{ b(z) w(r) j_l(k_{ln'}r) j_l(k_{ln}) + \frac{\Omega_m^{0.6}(z)}{k_{ln'}^2} \frac{d}{dr} [w(r) j_l(k_{ln}r)] \frac{d}{dr} j_l(k_{ln'}r) \right\} r^2 dr, \quad (A4)$$

where σ_z is the photometric redshift error in comoving distance units, and $\Omega_m(z)$ is the ratio between the cosmic matter density to the critical density at redshift z . For simplicity, we have assumed a full-sky survey with no angular variation in the selection function, so that the galaxy distribution $n_g(\mathbf{r}) = \bar{n}_g(r)[b(z)g(z)\delta(\mathbf{r}) + 1]$, in which $\delta(\mathbf{r})$ is scaled to $z = 0$. The term $S_{lnn'}$ would account for the nonlinear redshift distortion, i.e. the pair-wise velocity dispersion, if there were no error in redshift measurements. Since the photometric redshift error is far greater than the pair-wise velocity dispersion, the latter is neglected. The term $Q_{lnn'}$ is due to the linear redshift distortion (for a better approximation, see Scoccimarro 2004). With $\langle \delta_{lmn} \delta_{l'm'n'}^* \rangle = P(k_{ln}) \delta_{ll'}^K \delta_{mm'}^K \delta_{nn'}^K$, one can show that

$$\langle |D_{ln}|^2 \rangle = \langle |D_{lmn}|^2 \rangle_m = \sum_{n'} U_{lnn'}^2 P(k_{ln'}) + N_{ln}, \quad (A5)$$

where the window function $U_{lnn'}^2$ and shot noise N_{ln} , respectively, are given by

$$U_{lnn'} = \sum_{n''} S_{lnn''} Q_{lnn''n'} \quad \text{and} \quad N_{ln} = c_{ln}^2 \int \bar{n}_g(r) w^2(r) j_l^2(k_{ln}r) r^2 dr. \quad (A6)$$

The weight function $w(r)$ is introduced in equation (A1) to reduce the variance in the power spectrum estimator. Designing an optimal weight function is beyond the scope of this work. Here, we only demonstrate the performance of the estimator with a commonly used weight function, $w(r) = P(k)/[1 + \bar{n}_g(r)P(k)]$ (Feldman et al. 1994). Fig. 5 shows several examples of the window function $U_{lnn'}^2$. The fiducial cosmological parameters are given by the *WMAP* results (Spergel et al. 2003), and the matter power spectrum is calculated using the fitting formula from Eisenstein & Hu (1999). We model the evolution of an overall bias with $b(z) = 0.84z + 1$ (e.g. Weinberg et al. 2004). The symbols mark the discrete wavenumbers of the radial modes. The window function $U_{lnn'}^2$ is fairly narrow for $k < 0.02 h \text{ Mpc}^{-1}$, except for $U_{l1n'}^2$ (not shown), which are discarded in the mode counting. The results of other multipoles share the same characteristics, except that for higher multipoles the modes move toward large wavenumbers and vice versa.

REFERENCES

Alcock, C. & Paczynski, B. 1979, *Nature*, 281, 358
 Angulo, R., Baugh, C. M., Frenk, C. S., Bower, R. G., Jenkins, A., & Morris, S. L. 2005, *MNRAS* in press (astro-ph/0504456)
 Babbedge, T. S. R., Whitaker, R., & Morris, S. 2005, *MNRAS* in press (astro-ph/0505108)
 Ballinger, W. E., Peacock, J. A., & Heavens, A. F. 1996, *MNRAS*, 282, 877
 Bennett, C. L. et al. 2003, *ApJS*, 148, 97
 Blake, C. & Bridle, S. 2004, submitted to *MNRAS* (astro-ph/0411713)
 Blake, C. & Glazebrook, K. 2003, *ApJ*, 594, 665
 Bond, J. R. & Efstathiou, G. 1984, *ApJ*, 285, L45
 Bridle, S. L., Lewis, A. M., Weller, J., & Efstathiou, G. 2003, *MNRAS*, 342, L72
 Burstein, D. 2003, *AJ*, 126, 1849
 Burstein, D. & Heiles, C. 1982, *AJ*, 87, 1165
 Cline, J. M., Crotty, P., & Lesgourgues, J. 2003, *Journal of Cosmology and Astro-Particle Physics*, 9, 10
 Cole, S., Fisher, K. B., & Weinberg, D. H. 1994, *MNRAS*, 267, 785
 Cole, S. et al. 2005, submitted to *MNRAS* (astro-ph/0501174)
 Contaldi, C. R., Peloso, M., Kofman, L., & Linde, A. 2003, *Journal of Cosmology and Astro-Particle Physics*, 7, 2
 Cooray, A., Hu, W., Huterer, D., & Joffre, M. 2001, *ApJ*, 557, L7
 de Oliveira-Costa, A., Tegmark, M., Zaldarriaga, M., & Hamilton, A. 2004, *Phys. Rev. D*, 69, 063516
 Dolney, D., Jain, B., & Takada, M. 2004, ArXiv Astrophysics e-prints (astro-ph/0409445)
 Doré, O., Holder, G. P., & Loeb, A. 2004, *ApJ*, 612, 81
 Efstathiou, G. 2004, *MNRAS*, 348, 885
 Eisenstein, D. J. & Hu, W. 1999, *ApJ*, 511, 5
 Eisenstein, D. J., Hu, W., & Tegmark, M. 1998, *ApJ*, 504, L57
 Eisenstein, D. J., Hu, W., & Tegmark, M. 1999, *ApJ*, 518, 2
 Eisenstein, D. J. et al. 2005, submitted to *ApJ* (astro-ph/0501171)
 Eriksen, H. K., Banday, A. J., Górski, K. M., & Lilje, P. B. 2004a, *ApJ*, 612, 633
 Eriksen, H. K., Hansen, F. K., Banday, A. J., Górski, K. M., & Lilje, P. B. 2004b, *ApJ*, 605, 14
 Feldman, H. A., Kaiser, N., & Peacock, J. A. 1994, *ApJ*, 426, 23
 Fisher, K. B., Scharf, C. A., & Lahav, O. 1994, *MNRAS*, 266, 219
 Gaztañaga, E., Wagg, J., Multamäki, T., Montaña, A., & Hughes, D. H. 2003, *MNRAS*, 346, 47
 Glazebrook, K. & Blake, C. 2005, *ApJ* in press, (astro-ph/0505608)
 Gottlöber, S., Müller, V., Starobinsky, A. A. 1991, *Phys. Rev. D*, 43, 2510
 Hajian, A., Souradeep, T., & Cornish, N. 2005, *ApJ*, 618, L63
 Hansen, F. K., Cabella, P., Marinucci, D., & Vittorio, N. 2004, *ApJ*, 607, L67
 Heavens, A. F. & Taylor, A. N. 1995, *MNRAS*, 275, 483
 Hoekstra, H., van Waerbeke, L., Gladders, M. D., Mellier, Y., & Yee, H. K. C. 2002, *ApJ*, 577, 604
 Holtzman, J. A. 1989, *ApJS*, 71, 1
 Hu, W. & Haiman, Z. 2003, *Phys. Rev. D*, 68, 063004
 Hu, W. & Jain, B. 2004, *Phys. Rev. D*, 70, 043009
 Hu, W. & Okamoto, T. 2004, *Phys. Rev. D*, 69, 043004
 Hu, W. & Sugiyama, N. 1996, *ApJ*, 471, 542
 Huterer, D., Takada, M., Bernstein, G., & Jain, B. 2005, submitted to *MNRAS* (astro-ph/0506030)
 Jaffe, T. R., Banday, A. J., Eriksen, H. K., Gorski, K. M., & Hansen, F. K. 2005, submitted to *ApJ* (astro-ph/0503213)
 Kaiser, N. 1987, *MNRAS*, 227, 1
 Kesden, M., Kamionkowski, M., & Cooray, A. 2003, *Phys. Rev. Lett.*, 91, 221302
 Lahav, O., Lilje, P. B., Primack, J. R., & Rees, M. J. 1991, *MNRAS*, 251, 128
 Land, K. & Magueijo, J. 2005, *MNRAS*, 357, 994
 Linder, E. V. 2003, *Phys. Rev. D*, 68, 083504
 Linder, E. V. 2005, ArXiv Astrophysics e-prints (astro-ph/0507308)
 Liske, J., Lemon, D. J., Driver, S. P., Cross, N. J. G., & Couch, W. J. 2003, *MNRAS*, 344, 307
 Luminet, J., Weeks, J. R., Riazuelo, A., Lehoucq, R., & Uzan, J. 2003, *Nature*, 425, 593
 Ma, Z., Hu, W., & Huterer, D. 2005, submitted to *ApJ* (astro-ph/0506614)
 Metcalfe, N., Shanks, T., Campos, A., McCracken, H. J., & Fong, R. 2001, *MNRAS*, 323, 795

Norberg, P. et al. 2001, MNRAS, 328, 64
 O'Dwyer, I. J. et al. 2004, ApJ, 617, L99
 Padmanabhan, N. et al. 2005, MNRAS, 359, 237
 Peacock, J. A. et al. 2001, Nature, 410, 169
 Peacock, J. A. & Smith, R. E. 2000, MNRAS, 318, 1144
 Peebles, P. J. E. & Yu, J. T. 1970, ApJ, 162, 815
 Peiris, H. V. et al. 2003, ApJS, 148, 213
 Pen, U. 2004, MNRAS, 350, 1445
 Percival, W. J. et al. 2004, MNRAS, 353, 1201
 Pozzetti, L., Madau, P., Zamorani, G., Ferguson, H. C., & Bruzual A., G. 1998, MNRAS, 298, 1133
 Scharf, C., Hoffman, Y., Lahav, O., & Lynden-Bell, D. 1992, MNRAS, 256, 229
 Schlegel, D. J., Finkbeiner, D. P., & Davis, M. 1998, ApJ, 500, 525
 Schwarz, D. J., Starkman, G. D., Huterer, D., & Copi, C. J. 2004, Phys. Rev. Lett., 93, 221301
 Scoccimarro, R. 2004, Phys. Rev. D, 70, 083007
 Seljak, U. et al. 2005, Phys. Rev. D, 71, 043511
 Seo, H. & Eisenstein, D. J. 2003, ApJ, 598, 720
 Seo, H. & Eisenstein, D. J. 2005, ApJ in press (astro-ph/0507338)
 Skordis, C. & Silk, J. 2004, astro-ph/0402474
 Slosar, A. & Seljak, U. 2004, Phys. Rev. D, 70, 083002
 Spergel, D. N. et al. 2003, ApJS, 148, 175
 Tadros, H. et al. 1999, MNRAS, 305, 527
 Tegmark, M. 1997, Physical Review Letters, 79, 3806
 Tegmark, M. et al. 2004, ApJ, 606, 702
 Tyson, J. A. 1988, AJ, 96, 1
 Weinberg, D. H., Davé, R., Katz, N., & Hernquist, L. 2004, ApJ, 601, 1
 White, M. 2005, ArXiv Astrophysics e-prints (astro-ph/0507307)
 Williams, R. E. et al. 1996, AJ, 112, 1335
 Yasuda, N. et al. 2001, AJ, 122, 1104
 Zehavi, I. et al. 2002, ApJ, 571, 172
 Zhan, H. & Fang, L. 2003, ApJ, 585, 12
 Zhan, H., & Knox, L. 2005, in preparation